The Astrophysical Journal Letters, 992:L2 (7pp), 2025 October 10 https://doi.org/10.3847/2041-8213/ae09a8

Discovery of an Accretion Burst in a Free-floating Planetary-mass Object

Victor Almendros-Abad[1], Aleks Scholz[2], Belinda Damian[2], Ray Jayawardhana[3], Amelia Bayo[4], Laura Flagg[3], Koraljka Mužić[5], Antonella Natta[6,7], Paola Pinilla[8], and Leonardo Testi[9]
[1] Istituto Nazionale di Astrofisica (INAF)—Osservatorio Astronomico di Palermo, Piazza del Parlamento 1, 90134, Palermo, Italy; victor.almendrosabad@inaf.it
[2] SUPA, School of Physics & Astronomy, University of St Andrews, North Haugh, St Andrews, KY16 9SS, UK
[3] Department of Physics & Astronomy, Johns Hopkins University, Baltimore, MD 21218, USA
[4] European Southern Observatory, Karl-Schwarzschild-Strasse 2, D-85748 Garching bei München, Germany
[5] Instituto de Astrofísica e Ciências do Espaço, Faculdade de Ciências, Universidade de Lisboa, Ed. C8, Campo Grande, 1749-016 Lisbon, Portugal
[6] School of Cosmic Physics, Dublin Institute for Advanced Studies, 31 Fitzwilliam Place, Dublin 2, Ireland
[7] University College Dublin (UCD), Department of Physics, Belfield, Dublin 4, Ireland
[8] Mullard Space Science Laboratory, University College London, Holmbury St Mary, Dorking, London, UK
[9] Dipartimento di Fisica e Astronomia, Università di Bologna, Via Gobetti 93/2, 40122, Bologna, Italy
Received 2025 August 29; revised 2025 September 18; accepted 2025 September 19; published 2025 October 2

Abstract

We report the discovery of a long-lasting burst of disk accretion in Cha J11070768-7626326 (Cha 1107-7626), a young, isolated, 5–10 $M_{\rm Jupiter}$ object. In spectra taken with XSHOOTER at ESO's Very Large Telescope as well as NIRSpec and MIRI on the James Webb Space Telescope, the object transitions from quiescence in 2025 April–May to a strongly enhanced accretion phase in 2025 June–August. The line flux changes correspond to a 6–8-fold increase in the mass accretion rate, reaching $10^{-7}\,M_{\rm Jupiter}{\rm yr}^{-1}$, the highest measured in a planetary-mass object. During the burst, the Hα line develops a double-peaked profile with redshifted absorption, as observed in stars and brown dwarfs undergoing magnetospheric accretion. The optical continuum increases by a factor of 3–6; the object is ∼1.5–2 mag brighter in the *R* band during the burst. Mid-infrared continuum fluxes rise by 10%–20%, with clear changes in the hydrocarbon emission lines from the disk. We detect water vapour emission at 6.5–7 μm, which were absent in quiescence. By the end of our observing campaign, the burst was still ongoing, implying a duration of at least 2 months. A 2016 spectrum also shows high accretion levels, suggesting that this object may undergo recurring bursts. The observed event is inconsistent with typical variability in accreting young stars and instead matches the duration, amplitude, and line spectrum of an EXor-type burst, making Cha1107-7626 the first substellar object with evidence of a potentially recurring EXor burst.

Unified Astronomy Thesaurus concepts: Stellar accretion disks (1579); Protoplanetary disks (1300); Brown dwarfs (185); Infrared spectroscopy (2285); Spectroscopy (1558); H I line emission (690); Young stellar objects (1834)

1. Introduction

Deep surveys in star-forming regions have identified young free-floating objects with masses below the deuterium burning limit at 13 Jupiter masses, or 0.013 $M_{\odot}$, starting with the pioneering studies by M. R. Zapatero Osorio et al. (2000) and P. W. Lucas & P. F. Roche (2000). In terms of their masses, these objects are comparable to giant planets. They share some features with planets, including atmospheric properties (M. Bonnefoy et al. 2014). In contrast to planets, they are found in isolation, not in orbit around a star, and harbor accreting disks at young ages (K. L. Luhman et al. 2005; R. Jayawardhana & V. D. Ivanov 2006). The existence of free-floating planetary-mass objects (FFPMOs) raises many fundamental questions. Are these the lowest-mass objects formed like stars? What is the low-mass limit for star formation? Or are these giant planets that have been ejected from their planetary systems? How does the ejection occur exactly? (A. Scholz et al. 2022; N. Miret-Roig 2023; A. B. Langeveld et al. 2024).

Observationally, the most obvious path to constraining the nature of FFPMOs is a detailed characterization of the objects and their environment. Here, the study of disks and accretion is particularly relevant. The presence of a disk and ongoing accretion is typically interpreted as a sign that the object shares a formation and early evolutionary path with stars. Disks have been found through infrared excess for objects with 5–10 Jupiter masses (L. Testi et al. 2002; K. L. Luhman et al. 2008). The disk fractions do not seem to decline in the planetary-mass domain (H. H. Seo & A. Scholz 2025). In some cases, evidence for gas accretion has been seen (G. Viswanath et al. 2024).

The object Cha1170-7626 is a key target in this regard—with an estimated mass of only 5–10 Jupiter masses, it is one of the lowest-mass FFPMOs with clear evidence for disk and accretion (K. L. Luhman et al. 2008). Recent observations with Very Large Telescope (VLT) and JWST have shown (a) clear evidence for infrared excess from 4 to 12 μm, (b) a silicate emission feature at 10 μm similar to those seen in stars and brown dwarfs, (c) hydrocarbon emission lines, indicating a carbon-rich disk chemistry, and (d) multiple accretion-induced emission lines (B. Damian et al. 2025; L. Flagg et al. 2025). These characteristics make Cha1107-7626 the poster child for disk accretion in the planetary-mass domain.

Using observations from VLT/XSHOOTER and instruments on board JWST, we recently discovered an accretion burst in Cha1107-7626, which began in 2025 June and was still ongoing by the end of 2025 August. This is the first time

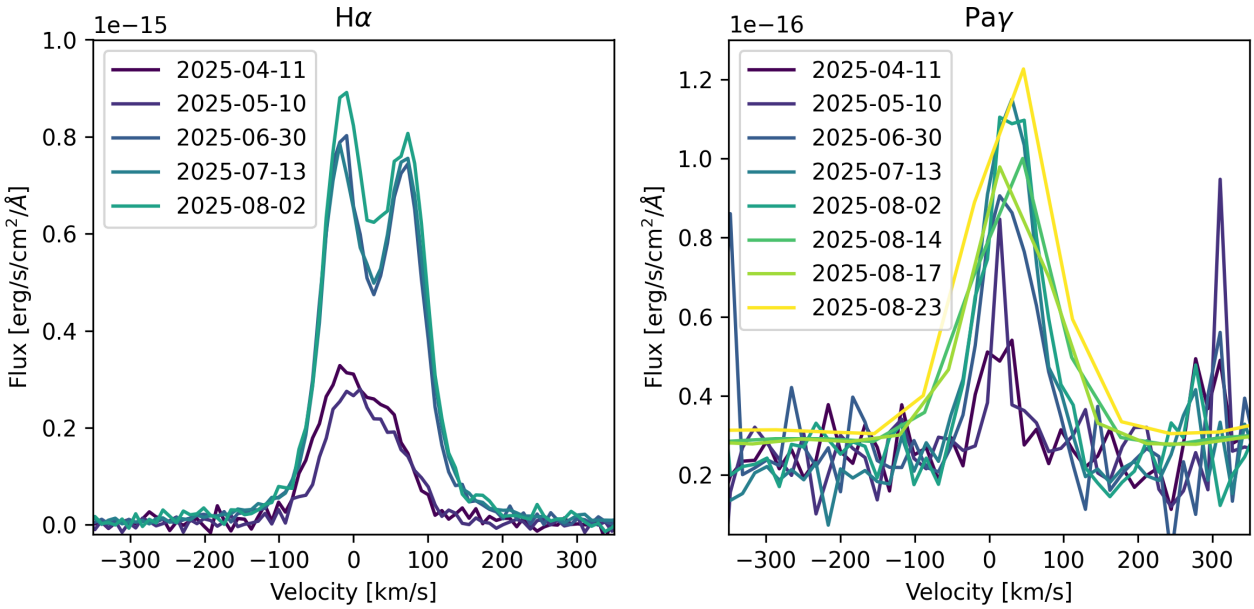

Figure 1. Line profile changes in Hα from VLT/XSHOOTER (left) and Paschen γ from both XSHOOTER and JWST (right) seen in VLT/XSHOOTER observations of Cha1107-7626. The eight epochs are color-coded and clearly show the evolution of the burst.

an accretion burst has been seen in an object with such a low mass. In Section 2, we present the observations and the resulting spectra. In Section 3, we analyze the changes in the accretion lines during the burst, derive the corresponding changes in mass accretion rate, and discuss the change in line profiles. In Section 4, we examine any changes in the broad spectral energy distribution in the optical, near- and mid-infrared. Our results are summarized in Section 5.

2. Observations

2.1. XSHOOTER

The burst was discovered as part of observations conducted with the XSHOOTER spectrograph on ESO's VLT (program 115.2850). Initially, three epochs were obtained, in April, May, and late 2025 June, the last one showing a clear increase in the strength of accretion-related emission lines. Two further epochs were obtained in mid July and early August in Director's Discretionary Time (programs 115.29FC and 115.29G3). All spectra were obtained under clear conditions except for the first, which ended with thick cloud conditions but yielded quality comparable to the second epoch. Seeing was $\leqslant 1\farcs1$ in all epochs except late 2025 June, when it was slightly worse.

XSHOOTER is a medium-resolution spectrograph that offers a very broad wavelength coverage from the ultraviolet to the near-infrared (NIR). All five observations used the same setup, with slit widths of $1\farcs0/0\farcs9/0\farcs9$ in the ultraviolet-blue (UVB)/visual-red (VIS)/NIR arms. Narrow-slit exposures were 600 s (UVB), 900 s (VIS), and 7×150 s (NIR), accompanied by $5''$ wide-slit exposures (10% of narrow-slit time) for slit-loss correction. In July and August, high airmass (>2.0) limited the observing window and prevented wide-slit observations. Data reduction was performed with the ESO XSHOOTER pipeline v.3.6.8 (A. Modigliani et al. 2010) with default settings, and telluric correction using Molecfit (A. Smette et al. 2015) v.4.4.2. Flux calibration was carried out by comparing the narrow-slit spectra to the corresponding wide-slit spectra in the first three epochs (J. M. Alcalá et al. 2017). The wide-slit fluxes were found to be consistent across these epochs within 10%. Since the observing conditions were similar for the 2025 June to August epochs, we used the wide-slit spectrum taken in June to also calibrate the 2025 July and August observations.

2.2. JWST

We observed Cha1107-7626 three times with JWST between 2025 August 14 and 22, using 9.7 hr of Director's Discretionary Time (program 9448). For each epoch, we used NIRSpec (P. Jakobsen et al. 2022) to obtain a low-resolution spectrum from 0.6 to 5.0 μm (with the PRISM setup) as well as medium-resolution spectra for two windows at 1.0–1.8 μm and 1.7–3.0 μm (using grisms G140H and G235H). In the first epoch, we also obtained a low-resolution spectrum (LRS) with MIRI (G. S. Wright et al. 2023) from 5 to 12 μm. The on-source times were 525 s for PRISM, 1838 s for the mid-resolution NIRSpec data, and 3591 s for MIRI-LRS. In the following, we used the pipeline-reduced data, which shows excellent consistency between setups. We also make use of the archival data for the same target obtained in 2024 August in program 4583 (B. Damian et al. 2025; L. Flagg et al. 2025). For the new PRISM and MIRI-LRS observations, we closely followed the configuration that was successfully used in the program from 2024.

3. Line Emission

3.1. Evolution of the Line Spectrum

The line spectrum for Cha1107-7626 shows a clear transition from a quiescent state to strongly enhanced accretion, which is sustained over several months. This is the hallmark of a long-lasting accretion burst (W. J. Fischer et al. 2023).

In Figure 1, we illustrate the evolution of two accretion-related emission lines through this event: Balmer Hα and

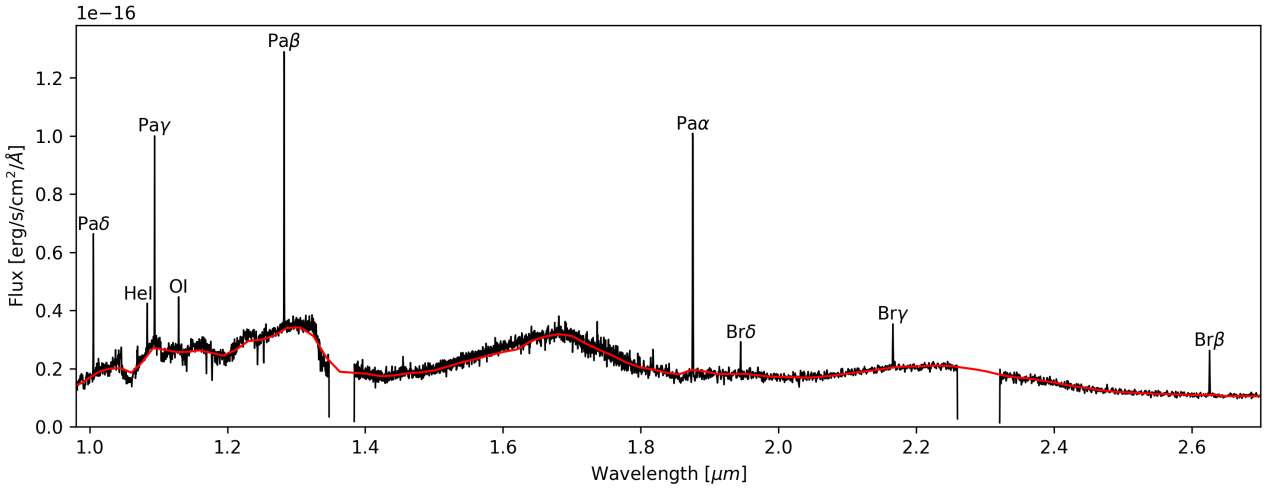

Figure 2. Medium-resolution G140H and G235H JWST NIRSpec spectra from 2025 August 14 (black line) together with the PRISM spectrum from the same epoch (red line). The strongest emission lines detected are identified.

Paschen γ. In 2025 April and May, Cha1107-7626 exhibits relatively weak accretion-related lines in the hydrogen Balmer and Paschen series. Between June and August, the emission line spectrum clearly strengthens. This is evident in the Hα line, which becomes broader, stronger, and also develops a double-peak profile, as seen in Figure 1. Such an enhancement in the emission line strength is also apparent when comparing NIRSpec/PRISM spectra from 2024 August and 2025 August, despite the very low resolution—the more recent observations exhibit a much stronger Hα (see Section 4.1).

Analogous changes are observed in other hydrogen lines. The Paschen γ line significantly increases in width and flux (Figure 1). In addition, lines not seen in April and May are visible in the June–August epochs, including Brackett γ, Paschen β, the calcium infrared triplet, and higher Paschen lines. The higher-resolution JWST/NIRSpec observations also reveal strong emission from Paschen α, Brackett β, and several higher Brackett and Pfund lines (Figure 2). The Balmer β line also strengthens in 2025 July and August. From 2025 June to August, the characteristics of the emission line spectrum show only minor changes.

3.2. Double-peaked Hα

The double-peaked, asymmetric Hα profile seen from 2025 June to August is in itself an exciting discovery. Such a profile is caused by absorption, superimposed onto the broad emission, shifted slightly to the red. In this particular case, the absorption trough is redshifted by 20–40 km s^{-1}. This type of line profile is a hallmark of funneled accretion seen at high inclination. The redshifted absorption is caused by cool, infalling gas in the accretion column, which is seen projected against the hot spot and causes the broad emission (J. Bouvier et al. 2003).

A very similar Hα profile change was observed in 2005 for the accreting brown dwarf TWA 27 (A. Scholz et al. 2005; A. Scholz & R. Jayawardhana 2006). In that case, the redshifted absorption was modulated on a rotational timescale. For Cha1107-7626, we do not have the high cadence data to check for this modulation. Similar to Cha1107-7626, the appearance of the double-peaked profile in TWA 27 was associated with a strong increase in the strength and width of the line. The profile changes in TWA 27 were interpreted as clear evidence for magnetically channeled accretion in substellar objects. The spectra for Cha1107-7626 presented in this Letter suggest that the same mode of accretion can be at work at objects with masses comparable to those of giant planets.

More specifically, we may observe a switch between two different accretion modes, for example, the stable/unstable modes suggested by R. Kurosawa & M. M. Romanova (2013). Stable accretion means that the configuration of the accretion columns is consistent over many rotational cycles. On the other hand, in the unstable mode, the accretion columns are variable on short timescales. This leads to enhanced accretion rates, as well as persistent redshifted absorption in lines—as observed in our target.

3.3. Accretion Rate Changes

The accretion luminosity at each epoch was estimated following the same method as L. Flagg et al. (2025), using established recipes. We adopted the photospheric parameters derived in B. Damian et al. (2025). In short, we measure the line luminosities on the dereddened spectra and convert to the total accretion luminosity using the empirical relations from J. M. Alcalá et al. (2017).

The evolution of the mass accretion rate from Hα and Paschen γ (i.e., the two lines detected across all XSHOOTER epochs) is shown in Figure 3. We also show the average accretion rate from several lines detected in the XSHOOTER and JWST observations: Hα, Paschen δ, Paschen γ, Paschen β, and Brackett γ. We note that Hα is not covered in the JWST grism spectra used for the accretion rate estimates, while Paschen δ, Paschen β, and Brackett γ are detected only during the enhanced accretion phase. Both the individual line tracers and the average indicate a sixfold increase (corresponding to $\sim$0.8 dex) between the quiescence and enhanced phases. We estimate that self-absorption in Hα during the elevated state lowers the measured accretion rate by 10%, implying a true increase closer to eightfold. While the errors in the accretion rates derived from individual tracers are substantial, they are primarily systematic, which means that our estimate of the change in mass accretion rate over time is robust, as further supported by the consistency among multiple lines. In the last

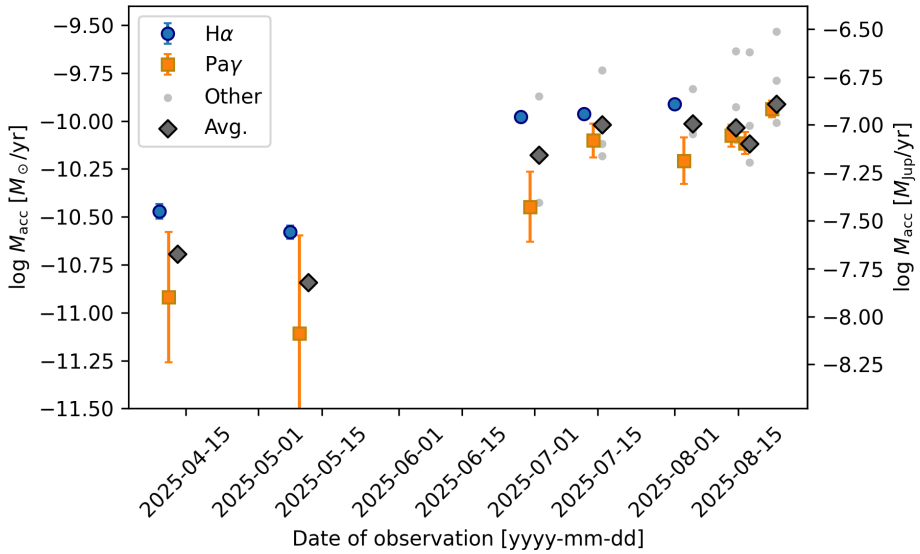

Figure 3. Time evolution of the mass accretion rate across all observations seen in Hα (blue circles) and Paschen γ (orange squares). Black diamonds show the average over the following available tracers at each epoch: Paschen δ, Paschen β, Brackett γ, and Hα, each shown with small light gray circles. A small offset in date has been applied for clarity. The Paγ and Hα accretion rate error bars represent the uncertainties from the line flux measurements only. Systematic uncertainties in the accretion rate, primarily from the adopted L_{line}–L_{acc} relation and stellar parameters, are not shown; these amount to $\sim$0.4 dex.

JWST epoch, we measure the strongest accretion rate, showing that the burst is still ongoing. This implies a duration of the burst of more than 2 months.

The accretion rate during the burst is $\sim 10^{-10}\,M_\odot \mathrm{yr}^{-1}$ or $10^{-7}\,M_{\mathrm{Jup}}\mathrm{yr}^{-1}$. This represents the strongest accretion rate measured on a planetary-mass object (see S. K. Betti et al. 2023). The only comparable measurement to our knowledge is that of OTS 44 derived from Paschen β (V. Joergens et al. 2013), which contrasts with the Hα measurement reported in the same Letter, that is 2 orders of magnitude lower. Those diagnostics were not obtained simultaneously, so the discrepancy may well be explained by strong accretion variability, similar to what we observe in Cha1107-7626. Compared to measured accretion rates in embedded protoplanets, the accretion rate in Cha1107-7626 during the burst is higher by at least a factor of $\sim$20 (L. M. Close et al. 2025).

The first two XSHOOTER epochs are consistent with the lower accretion rates measured from Hα (L. Flagg et al. 2025) in a 2008 optical spectrum (K. L. Luhman et al. 2008), which may represent the quiescent state. On the other hand, the XSHOOTER and JWST grism epochs from 2025 June to August match the accretion rates measured from Paschen β (L. Flagg et al. 2025) in a NIR spectrum taken in 2016 (V. Almendros-Abad et al. 2022). This suggests that events like the one reported here are recurring in this particular object, on timescales of years.

If we instead use line-accretion luminosity relations from "accretion-shock" models (Y. Aoyama et al. 2021), we obtain a similar temporal evolution, but the accretion rates in all epochs and lines are higher by about 1 order of magnitude. Thus, when adopting this specific model, the accretion rate during the burst is $10^{-9}\,M_\odot \mathrm{yr}^{-1}$ or $10^{-6}\,M_{\mathrm{Jup}}\mathrm{yr}^{-1}$.

4. Spectral Energy Distribution

4.1. Continuum

The JWST data from 2024 August and 2025 August provide us with an opportunity to probe the spectral energy distribution of Cha1107-7626 in quiescence and during the burst, over a wide wavelength range. In Figure 4, we show all available epochs observed with NIRSpec-PRISM and with MIRI-LRS. The object shows enhanced continuum emission during the accretion burst. In the optical and outside the Hα line, the flux levels are elevated by about a factor of 3–6 when comparing 2025 August to 2024 August. Combined with the increase in Hα, this would imply a photometric amplitude of about 1.5–2 mag in the R band. The additional continuum emission in this wavelength range likely originates from the accretion shock, so-called "veiling" (N. Calvet & E. Gullbring 1998). We note that such variations are not detected in the XSHOOTER spectra due to the low signal-to-noise ratio in the continuum at these wavelengths.

In the NIR range from 1–2 μm, the continuum emission remains approximately constant across all NIRSpec and XSHOOTER observations, with the exception of the last NIRSpec epoch, which shows increased fluxes by about 10%. At longer wavelengths, however, we see elevated flux levels by 10%–20% in all 2025 epochs, most strikingly between 5 and 10 μm. The straightforward explanation for the enhanced mid-infrared fluxes is an increase in the temperature of the inner disk, caused by the additional heating from the additional accretion (W. J. Fischer et al. 2023). Only a marginal temperature increase is needed for a 20% flux increase—assuming blackbody emission and typical inner disk temperatures of 500–1000 K, the required temperature increase is less than 100 K for the wavelength range in question.

The characteristic of the continuum changes is the expected consequence of an increase in the mass accretion rate; see the modeling in A. Scholz et al. (2013) for an exploration of this issue. For a moderate change in the accretion rate, the NIR fluxes remain almost unchanged. The optical flux, however, is strongly affected by the additional emission from the accretion shock, while the mid-infrared responds to the additional heating in the disk.

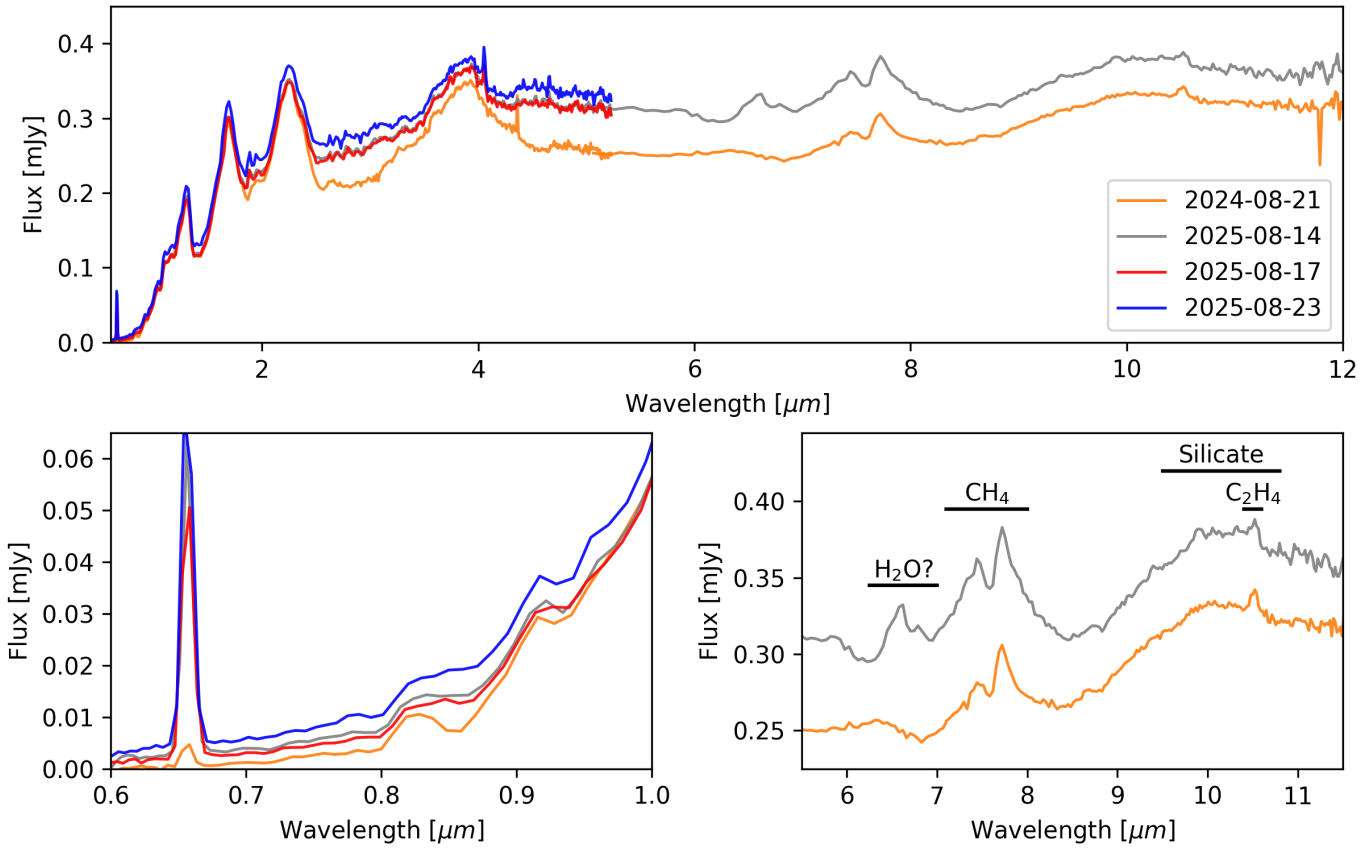

Figure 4. Time evolution of the spectral energy distribution for Cha1107-7626, as observed with JWST NIRSpec-PRISM and MIRI-LRS, in 2024 August and 2025 August. Bottom left and right panels show a zoom to the optical and mid-infrared, respectively. The main mid-infrared features discussed in Section 4 are indicated in the bottom right panel.

4.2. Hydrocarbon Lines

As reported by L. Flagg et al. (2025), Cha1107-7626 shows clear hydrocarbon emission lines originating in the disk in its quiescent mid-infrared spectrum. In particular, emission from CH_4 at 7–8 μm and C_2H_4 at 10.5 μm was identified based on the 2024 JWST data. The new MIRI data from 2025 August shows again both features, confirming that this is a carbon-rich disk.

Interestingly, we observe clear changes in the molecular line spectrum compared to quiescence. The double-peaked feature at 7–8 μm has changed in shape; in the new spectrum, the blue peak has increased in strength relative to the red one. In addition to these hydrocarbon lines, the burst spectrum shows a feature around 6.6 μm, which was not visible in quiescence (bottom right panel Figure 4). The emission is just beyond the 6.3 μm absorption caused by photospheric water (M. C. Cushing et al. 2006). A similarly shaped 6.6 μm feature has been reported in Spitzer spectra of accreting low-mass stars and was attributed to water vapor (B. A. Sargent et al. 2014). More subtle excesses in the same wavelength region have also recently been associated with water vapor in JWST/MIRI spectra of very low-mass stars and a substellar object (C. Xie et al. 2023; A. M. Arabhavi et al. 2025; M. Morales-Calderón et al. 2025). The strongest rovibrational H_2O bands predicted for accreting young stars are located near this wavelength (A. Banzatti et al. 2025), and increased H_2O emission has been observed during accretion bursts in EX Lupi (S. A. Smith et al. 2025). While we note that C_2H_6 also has transitions in this spectral region (T. Henning et al. 2024), the empirical evidence and the physical context of an accretion-driven temperature increase both favor an H_2O origin. We therefore identify the 6.6 μm feature as water vapor. This is the first time the chemical changes in the disk caused by increased accretion have been observed in a substellar object.

4.3. Silicate Feature

Cha1107-7626 exhibits a clear silicate feature at 8–10 μm, likely caused by a mix of small amorphous as well as crystallized grains (B. Damian et al. 2025). By eye, the shape of the silicate feature in 2025 is very similar to 2024. We calculated the standard metrics to quantify the strength and shape of the silicate feature, after dereddening, as shown in B. Damian et al. (2025). In 2024, the peak-over-continuum ratio at 10 μm was 1.2 ± 0.05, while the continuum-normalized flux ratio at between 11.3 and 9.8 μm was 0.87 ± 0.03. For comparison, the numbers for the 2025 August spectrum are 1.18 ± 0.05 and 0.88 ± 0.03. This shows that the strength and shape of the silicate feature before and during the burst are very similar.

For reference, strong changes in the silicate feature have been observed during accretion bursts for T Tauri stars. In particular, for EX Lupi, the silicate feature showed notable changes when observed 2 months after the peak of the outburst in 2008, compared to quiescence (P. Ábrahám et al. 2009; A. Juhász et al. 2012). While in quiescence, the silicate profile looked almost triangular, typical for interstellar medium-type grains; it became more complex and multipeaked during the

late stages of the outburst. The 2008 outburst of EX Lupi was an extreme event for this prototypical outbursting star, with a duration of 7 months, a brightness increase by 5 mag, and accretion rate changes by a factor of 30 (C. Aspin et al. 2010). It is therefore not directly comparable to the event reported here for Cha1107-7626.

5. Summary and Outlook

In this Letter, we present clear evidence for a significant accretion burst in the FFPMO Cha1107-7626. We use spectroscopic data from VLT/XSHOOTER and from instruments on board JWST to follow the evolution of the burst. Starting in late 2025 June, the object exhibits enhanced line emission compared to previous epochs, including a much stronger Hα feature. The Hα line is double-peaked with redshifted absorption, a hallmark for channeled, magnetospheric accretion. From the changes in hydrogen lines, we infer an increase in the mass accretion rate by a factor of 6–8 (corresponding to $\sim$0.8–0.9 dex).

The optical continuum is elevated by a factor of 3–6 compared to quiescence. The NIR remains largely unchanged except for a $\sim$10% increase in the final epoch, and the mid-infrared fluxes are enhanced by 10%–20%. While the silicate feature is effectively unchanged, we report clear changes in the hydrocarbon line spectrum during the burst, in particular the appearance of a feature at 6.6 μm attributed to water vapor. By the end of 2025 August, the accretion burst is still ongoing and in fact shows the strongest accretion rates measured, mirrored by the strongest Hα and optical continuum excess. This implies that the burst has lasted for more than 2 months, though its true duration remains unconstrained. The archival spectra for Cha1107-7626 indicate that a similar event may have happened about 10 years ago.

Accretion variability is commonly observed in young stars and has also been documented in substellar objects, including those with planetary masses (G. Viswanath et al. 2024). For typical young stars, however, accretion rate changes do not exceed a factor of $\sim$3 on timescales of days to months (D. C. Nguyen et al. 2009). Cha1107-7626 clearly shows unusually strong accretion variability compared to these typical cases. The duration of the observed event also distinguishes it from the most common variability of T Tauri stars, whose timescale is controlled by the stellar rotation (G. Costigan et al. 2012, 2014). While the rotation period of Cha1107-7626 is not known, it can be expected to be in the range of 1–4 days (A. Scholz et al. 2018), which means that the accretion event lasted more than 15 rotational cycles.

On the other hand, the observed event seen in Cha1107-7626 is comparable to EXor-type bursts, considering its duration, the optical amplitude, accretion rate increase, and the changes in the line spectrum (A. Sicilia-Aguilar et al. 2012; W. J. Fischer et al. 2023). As an example, the 2022 burst of the prototype EX Lupi lasted about 4 months. At its peak, the star was brightened by 2 mag in the optical, with an increase in mass accretion by a factor of 7 (F. Cruz-Sáenz de Miera et al. 2023; K. Singh et al. 2024). The event observed for Cha1107-7626 shows very similar characteristics. Cha1107-7626 is therefore the first planetary-mass object identified as an EXor, extending this class of bursts to the regime of giant planets.

These kinds of accretion bursts are key events in the early evolution of stars (M. Audard et al. 2014; W. J. Fischer et al. 2023). In particular, such events can have a significant effect on the chemical and physical evolution of the disk (P. Ábrahám et al. 2009; S. A. Smith et al. 2025) and potentially on the early stages of planet formation. Our target is the lowest mass object observed thus far that is going through an accretion burst, and by far the lowest in the EXor category. Detailed studies of accretion variability have, in the past, helped to illuminate the interactions between young stellar objects and their disks, including the role of magnetic fields. Similarly, the observations presented here provide a glimpse into the nature of accretion in planetary-mass objects.

Acknowledgments

We thank John Pritchard and Paula Sanchez Saez at ESO for their support during the preparation and execution of the XSHOOTER observations. We also thank Weston Eck, Tony Keyes, and Greg Sloan at the Space Telescope Science Institute for their assistance with the JWST observations. V.A.A. acknowledges support from the INAF grants 1.05.12.05.03 and 1.05.24.07.02. A.S. and B.D. acknowledge support from the UKRI Science and Technology Facilities Council through grant ST/Y001419/1/. A.B. acknowledges support from the Deutsche Forschungsgemeinschaft (DFG, German Research Foundation) under Germany's Excellence Strategy—EXC 2094—390783311. K.M. acknowledges support from the Fundação para a Ciência e a Tecnologia (FCT) through the grant 2022.03809.CEECIND. P.P. acknowledges funding from the UK Research and Innovation (UKRI) under the UK government's Horizon Europe funding guarantee from ERC (under grant agreement No. 101076489).

Based on observations collected at the European Southern Observatory under programmes 115.2850, 115.29FC, and 115.29G3. This work is based (in part) on observations made with the NASA/ESA/CSA James Webb Space Telescope. The data were obtained from the Mikulski Archive for Space Telescopes at the Space Telescope Science Institute, which is operated by the Association of Universities for Research in Astronomy, Inc., under NASA contract NAS 5-03127 for JWST. These observations are associated with programs #4583 and #9488. The specific observations analyzed can be accessed via doi:10.17909/jfng-v154.

Facilities: JWST, VLT:Melipal.

Software: EsoReflex (W. Freudling et al. 2013), Molecfit (A. Smette et al. 2015), Astropy (Astropy Collaboration et al. 2013, 2018, 2022), Matplotlib (J. D. Hunter 2007), NumPy (C. R. Harris et al. 2020), SciPy (P. Virtanen et al. 2020).

ORCID iDs

Victor Almendros-Abad https://orcid.org/0000-0002-4945-9483
Aleks Scholz https://orcid.org/0000-0001-8993-5053
Belinda Damian https://orcid.org/0000-0002-2234-4678
Ray Jayawardhana https://orcid.org/0000-0001-5349-6853
Amelia Bayo https://orcid.org/0000-0001-7868-7031
Laura Flagg https://orcid.org/0000-0001-6362-0571
Koraljka Mužić https://orcid.org/0000-0002-7989-2595
Antonella Natta https://orcid.org/0000-0002-4608-7995
Paola Pinilla https://orcid.org/0000-0001-8764-1780
Leonardo Testi https://orcid.org/0000-0003-1859-3070

References

Ábrahám, P., Juhász, A., Dullemond, C. P., et al. 2009, Natur, 459, 224
Alcalá, J. M., Manara, C. F., Natta, A., et al. 2017, A&A, 600, A20

Almendros-Abad, V., Mužić, K., Moitinho, A., Krone-Martins, A., & Kubiak, K. 2022, A&A, 657, A129
Aoyama, Y., Marleau, G.-D., Ikoma, M., & Mordasini, C. 2021, ApJL, 917, L30
Arabhavi, A. M., Kamp, I., van Dishoeck, E. F., et al. 2025, ApJL, 984, L62
Aspin, C., Reipurth, B., Herczeg, G. J., & Capak, P. 2010, ApJL, 719, L50
Astropy Collaboration, Price-Whelan, A. M., Lim, P. L., et al. 2022, ApJ, 935, 167
Astropy Collaboration, Price-Whelan, A. M., Sipőcz, B. M., et al. 2018, AJ, 156, 123
Astropy Collaboration, Robitaille, T. P., Tollerud, E. J., et al. 2013, A&A, 558, A33
Audard, M., Ábrahám, P., Dunham, M. M., et al. 2014, in Protostars and Planets VI, ed. H. Beuther et al. (Tucson, AZ: Univ. Arizona Press), 387
Banzatti, A., Salyk, C., Pontoppidan, K. M., et al. 2025, AJ, 169, 165
Betti, S. K., Follette, K. B., Ward-Duong, K., et al. 2023, AJ, 166, 262
Bonnefoy, M., Chauvin, G., Lagrange, A. M., et al. 2014, A&A, 562, A127
Bouvier, J., Grankin, K. N., Alencar, S. H. P., et al. 2003, A&A, 409, 169
Calvet, N., & Gullbring, E. 1998, ApJ, 509, 802
Close, L. M., van Capelleveen, R. F., Weible, G., et al. 2025, ApJL, 990, L9
Costigan, G., Scholz, A., Stelzer, B., et al. 2012, MNRAS, 427, 1344
Costigan, G., Vink, J. S., Scholz, A., Ray, T., & Testi, L. 2014, MNRAS, 440, 3444
Cruz-Sáenz de Miera, F., Kóspál, Á., Abrahám, P., et al. 2023, A&A, 678, A88
Cushing, M. C., Roellig, T. L., Marley, M. S., et al. 2006, ApJ, 648, 614
Damian, B., Scholz, A., Jayawardhana, R., et al. 2025, AJ, 170, 127
Fischer, W. J., Hillenbrand, L. A., Herczeg, G. J., et al. 2023, in ASP Conf. Ser. 534, Protostars and Planets VII, ed. S.-i. Inutsuka et al. (San Francisco, CA: ASP), 355
Flagg, L., Scholz, A., Almendros-Abad, V., et al. 2025, ApJ, 986, 200
Freudling, W., Romaniello, M., Bramich, D. M., et al. 2013, A&A, 559, A96
Harris, C. R., Millman, K. J., van der Walt, S. J., et al. 2020, Natur, 585, 357
Henning, T., Kamp, I., Samland, M., et al. 2024, PASP, 136, 054302
Hunter, J. D. 2007, CSE, 9, 90
Jakobsen, P., Ferruit, P., Alves de Oliveira, C., et al. 2022, A&A, 661, A80
Jayawardhana, R., & Ivanov, V. D. 2006, ApJL, 647, L167
Joergens, V., Bonnefoy, M., Liu, Y., et al. 2013, A&A, 558, L7
Juhász, A., Dullemond, C. P., van Boekel, R., et al. 2012, ApJ, 744, 118
Kurosawa, R., & Romanova, M. M. 2013, MNRAS, 431, 2673
Langeveld, A. B., Scholz, A., Mužić, K., et al. 2024, AJ, 168, 179
Lucas, P. W., & Roche, P. F. 2000, MNRAS, 314, 858
Luhman, K. L., Adame, L., D'Alessio, P., et al. 2005, ApJL, 635, L93
Luhman, K. L., Allen, L. E., Allen, P. R., et al. 2008, ApJ, 675, 1375
Miret-Roig, N. 2023, Ap&SS, 368, 17
Modigliani, A., Goldoni, P., Royer, F., et al. 2010, Proc. SPIE, 7737, 773728
Morales-Calderón, M., Jang, H., Arabhavi, A. M., et al. 2025, arXiv:2508.05155
Nguyen, D. C., Scholz, A., van Kerkwijk, M. H., Jayawardhana, R., & Brandeker, A. 2009, ApJL, 694, L153
Sargent, B. A., Forrest, W., Watson, D. M., et al. 2014, ApJ, 792, 83
Scholz, A., Froebrich, D., & Wood, K. 2013, MNRAS, 430, 2910
Scholz, A., & Jayawardhana, R. 2006, ApJ, 638, 1056
Scholz, A., Jayawardhana, R., & Brandeker, A. 2005, ApJL, 629, L41
Scholz, A., Moore, K., Jayawardhana, R., et al. 2018, ApJ, 859, 153
Scholz, A., Muzic, K., Jayawardhana, R., Quinlan, L., & Wurster, J. 2022, PASP, 134, 104401
Seo, H. H., & Scholz, A. 2025, MNRAS, 537, 2579
Sicilia-Aguilar, A., Kóspál, Á., Setiawan, J., et al. 2012, A&A, 544, A93
Singh, K., Ninan, J. P., Romanova, M. M., et al. 2024, ApJ, 968, 88
Smette, A., Sana, H., Noll, S., et al. 2015, A&A, 576, A77
Smith, S. A., Romero-Mirza, C. E., Banzatti, A., et al. 2025, ApJL, 984, L51
Testi, L., Natta, A., Oliva, E., et al. 2002, ApJL, 571, L155
Virtanen, P., Gommers, R., Oliphant, T. E., et al. 2020, NatMe, 17, 261
Viswanath, G., Ringqvist, S. C., Demars, D., et al. 2024, A&A, 691, A64
Wright, G. S., Rieke, G. H., Glasse, A., et al. 2023, PASP, 135, 048003
Xie, C., Pascucci, I., Long, F., et al. 2023, ApJL, 959, L25
Zapatero Osorio, M. R., Béjar, V. J. S., Martín, E. L., et al. 2000, Sci, 290, 103